

Nonmonotonic dependence of comb polymer relaxation on branch density in semidilute solutions of linear polymers

Shivani F. Patel ^{1,*} Charles D. Young ^{1,*} Charles E. Sing,¹ and Charles M. Schroeder^{1,2,†}

¹*Department of Chemical and Biomolecular Engineering and Beckman Institute for Advanced Science and Technology, University of Illinois at Urbana-Champaign, Urbana, Illinois 61801, USA*

²*Department of Materials Science and Engineering, University of Illinois at Urbana-Champaign, Urbana, Illinois 61801, USA*



(Received 19 May 2020; revised 12 October 2020; accepted 20 November 2020; published 17 December 2020)

The dynamics of branched polymers in semidilute solutions are thought to depend on a coupling between polymer chain architecture, intermolecular excluded volume interactions, and long-range hydrodynamic interactions (HI). However, it has been challenging to quantitatively understand these phenomena due to the influence of intra- and intermolecular HI and chain-chain interactions for nonlinear polymer topologies in flow. In this work, we directly observe the relaxation dynamics of comb-shaped polymers in semidilute solutions of linear polymers using single molecule experiments and molecular simulations. Experimental results are directly complemented by coarse-grained simulations of comb polymers in semidilute solutions of linear polymers including long-range HI and excluded volume interactions. Our results show an unexpected nonmonotonic dependence of comb polymer relaxation time on branch density that arises due to a subtle yet important interplay between hydrodynamic shielding and polymer architecture.

DOI: [10.1103/PhysRevFluids.5.121301](https://doi.org/10.1103/PhysRevFluids.5.121301)

Branched polymers exhibit complex flow behavior due to nonlinear chain architectures [1]. The dynamics of branched polymers are qualitatively different than linear chains due to the presence of branch points [2]. In concentrated solutions and melts, linear polymers are known to topologically entangle and relax stress by reptation, which involves the snakelike motion of chains along the backbone contour [3]. However, branch points significantly slow down the relaxation of comb-shaped polymers [4], giving rise to hierarchical relaxation mechanisms that differ from those in linear polymer melts [5]. Such behavior gives rise to distinct rheological responses such as enhanced strain hardening together with shear thinning [6,7], unique linear viscoelastic signatures [8,9], and double stress overshoots in the startup of shear [10,11].

Branched polymer solutions are extensively used in applications such as consumer care products [12,13]. Moreover, nondilute solutions of branched polymers have been used for chemical sensing [14], optically active materials [15], and in emerging technologies such as three-dimensional printing [16]. Despite the utility of branched polymers, we lack a complete understanding of their dynamics in semidilute unentangled solutions, wherein polymer coils interpenetrate but do not topologically entangle [3]. In dilute polymer solutions, bulk properties arise from single isolated chain behavior, whereas in highly entangled concentrated solutions and melts, hydrodynamic interactions (HI) are screened and interchain interactions can be described using a mean-field approach [3]. In

*These authors contributed equally to this work.

†cms@illinois.edu

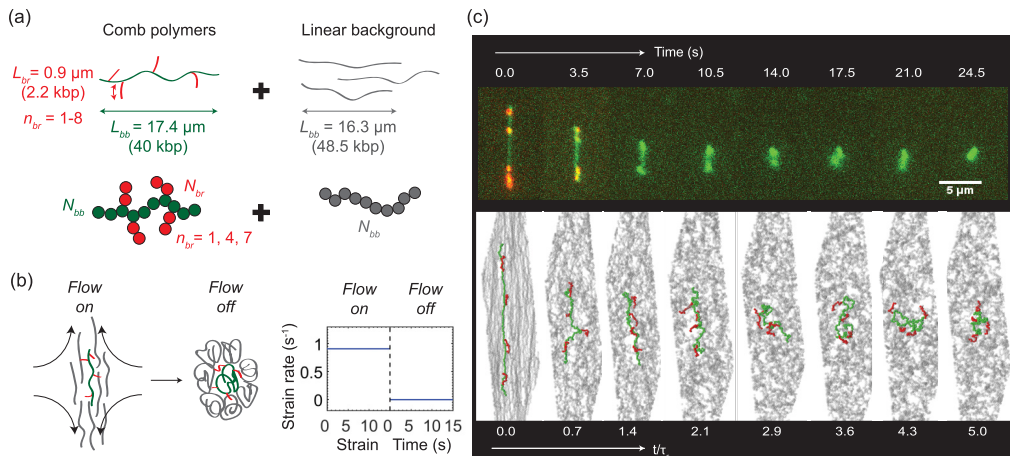


FIG. 1. Single molecule experiments and Brownian dynamics (BD) simulations of comb polymer relaxation in semidilute solutions. (a) Schematic of experimental system (top) showing dual-labeled comb polymers with backbones ($L_{bb} = 17.4 \mu\text{m}$) and branches ($L_{br} = 0.9 \mu\text{m}$) and (bottom) molecular model for BD simulations. (b) Schematic of relaxation experiment. (c) Top: Single molecule snapshots of a comb polymer with $n_{br} = 5$ branches relaxing after flow cessation. The red laser is turned off for $t \geq 4$ s to minimize photobleaching. Bottom: Snapshots from BD simulations showing comb relaxation ($n_{br} = 4$, green/red) in a background of semidilute linear polymers (gray) at equivalent time intervals as the experiment.

semidilute solutions, however, polymer dynamics are particularly challenging to understand due to the interplay between long-range HI, concentration fluctuations, and excluded volume interactions. These phenomena are further complicated by nonlinear chain architectures, which motivates the need to understand the role of branching on polymer dynamics in semidilute solutions.

In recent years, single molecule fluorescence microscopy has been used to directly observe polymer dynamics at the level of individual chains [17], enabling systematic studies in well-defined flows [18,19]. Concurrently, Brownian dynamics (BD) simulations have been used to probe the molecular origins of polymer flow behavior [20–22]. Single molecule experiments and BD simulations have yielded new insights into the dynamics of architecturally complex polymers such as combs [23,24], knots [25,26], and rings [27,28], mainly in dilute solutions. These approaches have also been extended to semidilute solutions, though prior work has focused on linear polymers [19,29–31].

In this work, we use single molecule fluorescence microscopy and BD simulations to understand the role of branching on polymer relaxation in semidilute solutions. Here, we directly visualize the relaxation dynamics of fluorescently labeled DNA comb polymers as a function of branching density in semidilute solutions of linear chains. Our results show an unexpected nonmonotonic dependence of comb polymer relaxation time on branch density, which is modeled using BD simulations of semidilute solutions with and without HI. BD simulations are performed across a wide range of branch density, branch lengths, and polymer concentrations, providing key insight into the molecular origins of the unexpected relaxation behavior of comb polymers. Taken together, our results show that comb polymer relaxation in semidilute solutions is governed by a complex interplay between long-range HI and polymer architecture.

DNA-based comb polymers were synthesized using a hybrid enzymatic-synthetic approach, as previously described (Fig. 1) [23,32,33]. Briefly, polymerase chain reaction (PCR) is used to generate the comb polymer backbones and branches with desired monodisperse lengths in separate reactions. Backbones ($M_{bb} = 40$ kbp) are synthesized with non-natural nucleotides enabling a graft-onto reaction for side branches via “click” (azide-alkyne) reaction. Branches ($M_{br} = 2.2$ kbp) are

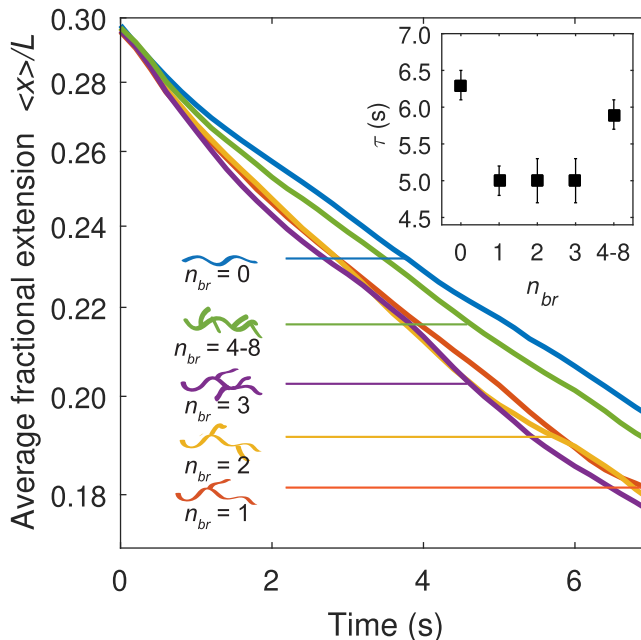


FIG. 2. Relaxation of comb polymers in semidilute solutions of linear chains. Ensemble-averaged relaxation trajectories of comb polymers from experiments ($M_{bb} = 40$ kbp, $M_{br} = 2$ kbp) as a function of branch number n_{br} compared to their linear analogs ($M_{bb} = 40$ kbp).

synthesized by incorporating Cy5 dye (red emission) during PCR, together with a single chemical group (azide) at one terminus enabling the graft-onto reaction. Following synthesis and purification, comb polymers are labeled with YOYO-1 dye (green emission), thereby allowing for simultaneous two-color imaging [23].

Polymer solutions are prepared by adding trace amounts of combs to semidilute unentangled solutions of linear polymers [Fig. 1(a)]. The unlabeled background solution consists of monodisperse linear DNA (λ -phage DNA, $M_{bb,\lambda} = 48.5$ kbp) at a concentration $c = 1 c^* = 50$ ng/ μ l, where c^* is the overlap concentration that defines the crossover from the dilute to the semidilute regime [30]. Comb polymers are added at an extremely low concentration corresponding to $c \approx 10^{-5}c^*$ relative to the linear polymer background. The contour lengths of fluorescently labeled comb backbones and branches are $L_{bb} = 17.4$ μ m and $L_{br} = 0.9$ μ m, respectively, with a persistence length $l_p = 56$ nm [17]. The contour lengths of the labeled comb backbone L_{bb} and unlabeled linear chains ($L = 16.3$ μ m, λ -phage DNA) are nearly equivalent [17].

We observed the relaxation of comb polymers following a step strain deformation in extensional flow [Figs. 1(b) and 1(c)]. During stretching, single comb polymers are trapped near the stagnation point in planar extensional flow using an automated flow control device known as the Stokes trap [34–38]. In this way, comb polymers are stretched to high degrees of extension (≈ 0.6 – $0.7L_{bb}$) for a time duration t using strain rates $\dot{\epsilon}$ above the coil-stretch transition for large fluid strains $\epsilon = \dot{\epsilon}t \approx 12$ – 15 . Prior to flow cessation, the number of branches on individual comb polymers is directly counted. Using this approach, we characterized the relaxation of comb polymers ($n_{br} \geq 1$ branches) and linear polymers ($n_{br} = 0$ branches) as a function of branching density (Fig. 2 and Supplemental Material Fig. S1 [32]). Here, we constructed separate molecular ensembles for different polymer architectures, including molecular ensembles for the cases of $n_{br} = 0, 1, 2, 3$ branches, and a combined molecular ensemble for $n_{br} = 4-8$. Ensemble-averaged trajectories from experiments for different

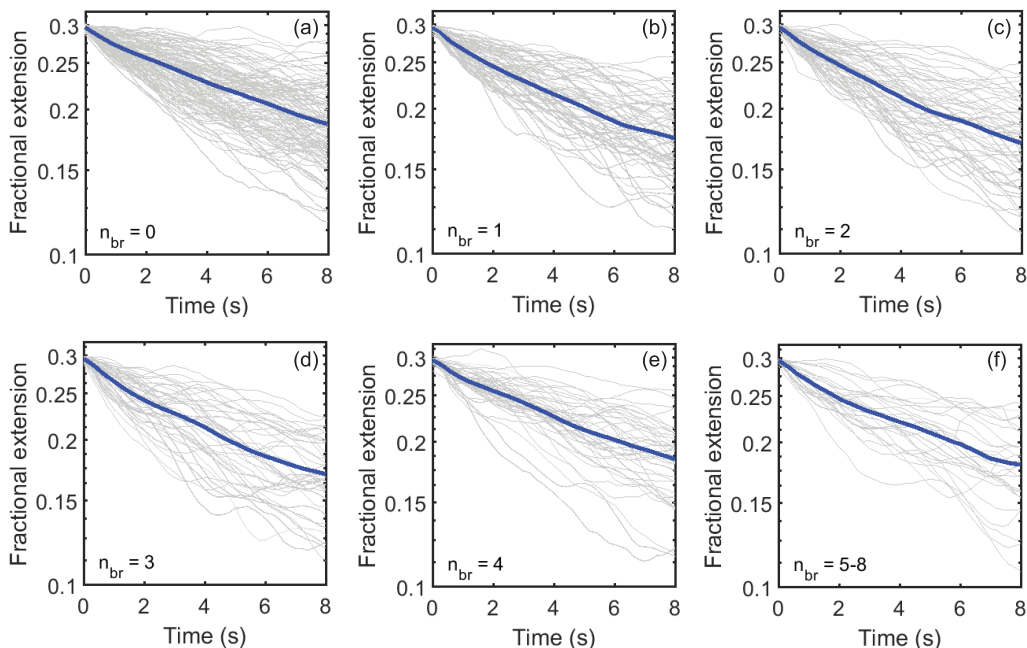


FIG. 3. Molecular ensembles of comb polymer relaxation as a function of the number of branches n_{br} from experiments. (a)–(f) Relaxation dynamics of DNA comb polymers in semidilute $1c^*$ solutions of linear chains following cessation of extensional flow. Relaxation dynamics are shown by plotting the fractional extension as a function of time for each branching density ($n_{br} = 0, 1, 2, 3, 4, 5-8$). Individual relaxation trajectories are shown in gray and the ensemble-averaged trajectories are shown in blue.

branching densities are shown in Fig. 2. Each ensemble contains at least 50 molecular trajectories, as shown in Fig. 3.

Relaxation times are quantified by tracking the polymer backbone stretch x as a function of time during the relaxation step, where x is the extent of the chain stretch in the flow plane. Here, we focus on the longest relaxation time corresponding to the linear entropic force regime [39], where the polymer fractional extension is $x/L < 0.3$. In dilute and semidilute unentangled solutions, the relaxation trajectories for linear polymers are well described by a single exponential decay for $x/L < 0.3$, such that $(x/L)^2 = A \exp(-t/\tau) + B$, where τ is the longest relaxation time and A and B are fitting constants [30]. Our results show that the relaxation trajectories for comb polymers in semidilute solutions of linear chains are well described by a single exponential (Supplemental Material Fig. S2), as shown previously for combs in dilute solution (Supplemental Material Fig. S3) [23].

The ensemble-averaged relaxation time for linear chains ($n_{br} = 0$) is $\tau = 6.3 \pm 0.2$ s. The average relaxation times for comb polymers with low branching density ($n_{br} = 1, 2, 3$) were found to be similar with $\tau = 5.0 \pm 0.3$ s. As branch density increases ($n_{br} \geq 4$), comb relaxation time increases such that $\tau = 5.9 \pm 0.2$ s. Error bars are determined as the standard error of the mean from individual trajectories and represent statistical variations arising from stochastic single molecule dynamics.

Unexpectedly, our results for comb polymer relaxation (Fig. 2, inset) show that comb polymers with a small number of branches ($n_{br} = 1, 2, 3$) relax faster than linear polymers ($n_{br} = 0$) in semidilute solutions. However, increasing the number of branches on comb polymers ($n_{br} \geq 4$) slows down the relaxation dynamics. These results are statistically significant such that differences in the ensemble-averaged relaxation times are larger than the standard error in molecular ensembles (Fig. 2, inset). This nonmonotonic trend in comb polymer relaxation times as a function of branch

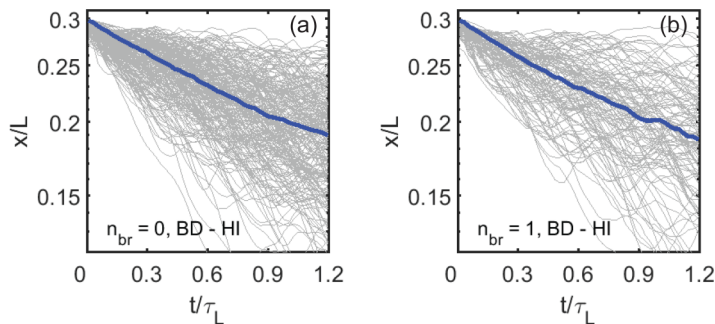


FIG. 4. Molecular ensembles of comb polymer relaxation as a function of the number of branches n_{br} from BD simulations with HI. Relaxation trajectories obtained from simulation for $N_{br} = 6$ for (a) $n_{br} = 0$ and (b) $n_{br} = 1$. Individual relaxation trajectories are shown in gray and the ensemble-averaged trajectories are shown in blue.

density is unexpected given that linear polymers relax faster than their comb counterparts in dilute solutions [23] and melts [7].

To understand the molecular origins of comb relaxation dynamics, we used BD simulations with HI. Here, polymers are modeled with $N_{bb} = 100$ backbone beads and $N_{br} = 6, 13,$ or 26 branch beads, connected by Kremer-Grest springs [32,40], and a varying number of branches $n_{br} = 0, 1, 4, 7$ [Fig. 1(a)]. In this model, the Kuhn step size is $l_K \approx 1.8\sigma$, where σ is the bead diameter. Comb backbones and branches in BD simulations have a proportionally smaller number of Kuhn segments compared to experiments, such that the ratio of backbone to branch length matches experiment ($M_{br}/M_{bb} \approx N_{br}/N_{bb}$). Intrachain and interchain HI is modeled using an Ewald sum Rotne-Prager-Yamakawa tensor [41,42]. BD simulations of nondilute solutions with HI are computationally demanding due to the calculation of HI and correlated Brownian noise; to accelerate the simulations, we use the iterative conformational averaging method [31,43,44], where the decomposition of the diffusion tensor is avoided by conformationally averaging the Brownian noise over transient polymer conformations [31,44]. In particular, the Brownian noise is determined by a conformationally averaged form of the truncated expansion ansatz introduced by Geyer and Winter [32,45]. Prior work has shown that such coarse-grained models successfully predict qualitative trends in experiments [27,31,44].

In an identical procedure to experiments, BD simulations are initialized with random polymer configurations and equilibrated for 10τ . A planar extensional flow is then applied using Kraynik-Reinelt boundary conditions [46,47] for an accumulated strain $\epsilon = 20$ – 25 at a flow strength $Wi > 1.5$, where $Wi = \dot{\epsilon}\tau$ is the dimensionless flow strength known as the Weissenberg number. In this way, polymers are stretched to a fractional extension $x/L > 0.5$, followed by abrupt flow cessation and relaxation of polymers to their equilibrium state (Fig. 4). During the relaxation step, the backbone end-to-end distance is tracked over time, enabling determination of the longest polymer relaxation times τ . Simulation ensembles contain 300 molecules, and error bars are determined from the standard error of four subsamples of the ensemble.

Figure 5(a) shows the longest relaxation times from experiments and BD simulations ($N_{br} = 6$). Here, relaxation times are nondimensionalized with the longest relaxation time of linear polymers (τ_L) to directly compare simulation and experiment. Both experiments and BD simulations with HI show the overall nonmonotonic dependence of polymer relaxation time on branch density. Compared to experimental data, BD simulations with $N_{br} = 6$ exhibit a smaller decrease in relaxation time between linear chains ($n_{br} = 0$) and combs with one branch ($n_{br} = 1$); we attribute this disparity to model coarse graining, because the nonmonotonicity becomes more pronounced with increasing branch length [$N_{br} = 6, 13,$ to 26 ; Fig. 5(b)]. Overall, BD simulations reveal that both interpolymer interactions and HI give rise to the nonmonotonic relaxation time. Increas-

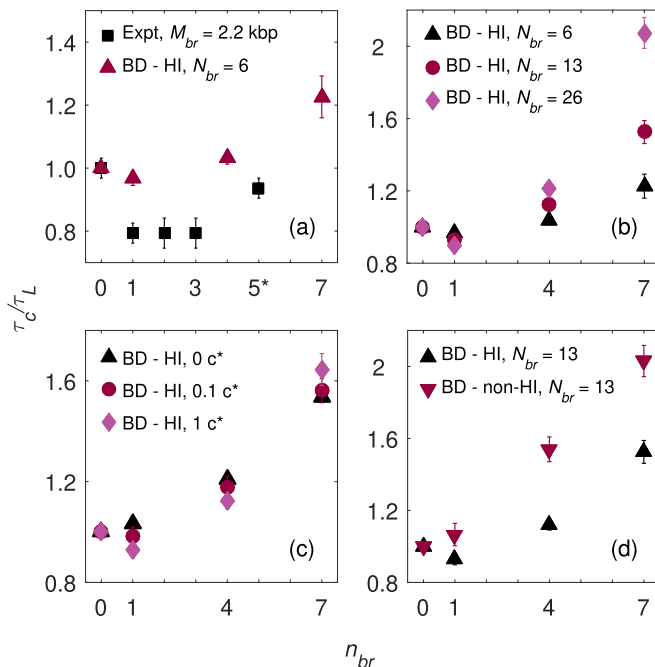


FIG. 5. Comb polymer relaxation time as a function of the number of branches n_{br} in semidilute solutions of linear polymers. (a) Normalized average relaxation time (τ_c/τ_L) of comb polymers from experiments (2.2 kbp branches) and simulations ($N_{br} = 6$). Molecular ensembles for comb polymers with $n_{br} \geq 4$ branches are combined and shown as $n_{br} = 5^*$. (b) Effect of branch size; scaled relaxation time for comb polymers in semidilute solutions from BD simulations with HI for branch sizes $N_{br} = 6, 13$, and 26 . (c) Effect of concentration; scaled relaxation time for comb polymers from BD simulations with HI in ultradilute and semidilute solutions at $0.1, 1.0c^*$. (d) Effect of HI; scaled relaxation time for comb polymers in semidilute solutions from BD simulations with and without HI for branch size $N_{br} = 13$.

ing concentration from $c = 0c^*$, $0.1c^*$, to $1.0c^*$ shows a smooth transition from a monotonic to nonmonotonic dependence of relaxation times on branching density [$N_{br} = 13$; Fig. 5(c)]. Figure 5(d) directly compares results from BD simulations with and without HI for $N_{br} = 13$ combs, showing that BD simulations without HI revert to a simple monotonic increase in the relaxation time.

Based on these results, we attribute the unusual relaxation behavior of comb polymers in semidilute solutions to an interplay between hydrodynamic screening and intermolecular excluded volume in nondilute polymer solutions. We hypothesize that comb polymer branches may induce a local dilution in the vicinity of their backbones due to steric interactions with nearby polymer chains in the background solution. To test this hypothesis, we performed BD simulations with and without HI for linear ($n_{br} = 0$, $N_{bb} = 100$) and comb polymers ($n_{br} = 1$, $N_{br} = 6, 13$, and 26 , $N_{bb} = 100$). We determined the equilibrium intermolecular radial distribution function $g(r)$ for a monomer located at a branch point for a comb with a single branch ($n_{br} = 1$) located in the center of the comb backbone (Fig. 6) or at different locations along the comb backbone (Fig. 7). For comparison, we also determined $g(r)$ for a monomer located in the center of a linear polymer backbone. At small distances r , neighboring polymers are depleted [$g(r) < 1$] due to steric interactions. Depletion is more significant for comb polymers, consistent with our hypothesis.

We quantify local dilution by determining a characteristic depletion distance ξ that is a proxy for the mesh size of a semidilute unentangled polymer solution. The depletion distance ξ is determined by relating the total number of depleted monomers $n_D = 4\pi \langle \rho \rangle \int_0^\infty r^2 [1 - g(r)] dr$ to an equivalent, fully depleted cavity of size ξ , $n_D = 4\pi \langle \rho \rangle \xi^3 / 3$, where $\langle \rho \rangle$ is the average monomer

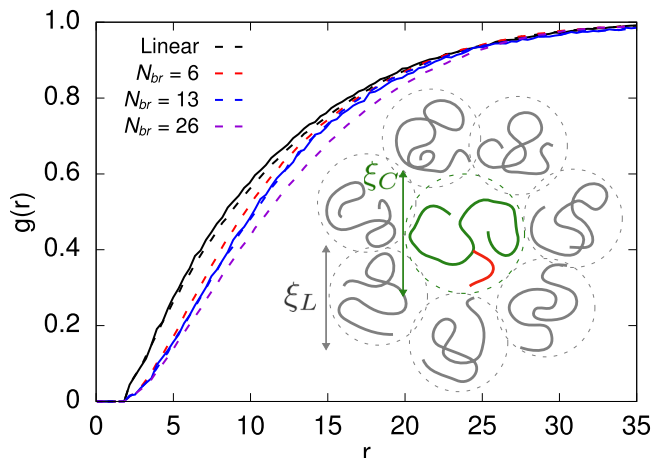


FIG. 6. Intermolecular radial distribution function for monomers at a backbone position $x_{br} = 0.5$ for linear polymers (black) and comb polymers with $N_{br} = 6$ (red), 13 (blue), and 26 (magenta) at $1.0c^*$. Results from simulations with HI (solid lines) and without HI (dashed lines) are shown. Inset: Schematic of correlation length for combs.

density. Equating the two expressions for n_D relates $g(r)$ to ξ . For the data shown in Fig. 6, we obtain the ratios $\xi_L/\xi_{C,6} = 0.991$, $\xi_L/\xi_{C,13} = 0.934$, and $\xi_L/\xi_{C,26} = 0.921$ for linear (L) to comb (C) polymers, where subscripts denote $N_{br} = 6, 13$, or 26. Scaling arguments for semidilute solutions assume that ξ is also a characteristic hydrodynamic screening length, relating polymer concentration ($\phi \propto \xi^{(1-3\nu)/\nu}$) to chain relaxation. Here, the longest polymer relaxation time in semidilute solutions is given by the scaling relation $\tau \propto \phi^{(2-3\nu)/(3\nu-1)}$, where ν is the solvent quality-dependent Flory exponent.

These relations can be combined to yield the ratio of comb to linear polymer relaxation times $\tau_C/\tau_L \simeq (\xi_L/\xi_C)^{(2-3\nu)/\nu}$. This expression is then used to estimate τ_C/τ_L , such that $\tau_{C,6}/\tau_L = 0.991$ and $\tau_{C,13}/\tau_L = 0.934$ for $\nu = 1/2$ and $\tau_{C,6}/\tau_L = 0.996$ and $\tau_{C,13}/\tau_L = 0.973$ for $\nu = 3/5$. For longer branches ($N_{br} = 26$), $\tau_{C,26}/\tau_L = 0.921$ for $\nu = 1/2$ and $\tau_{C,26}/\tau_L = 0.971$ for $\nu = 3/5$. Overall, these results are in reasonable agreement with the τ_C/τ_L values for the BD simulation results

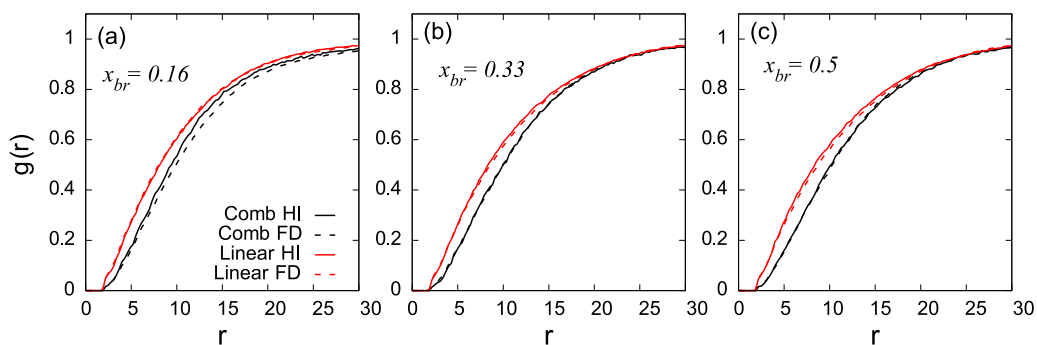


FIG. 7. Intermolecular radial distribution functions for a polymer bead at the branch point for a branch placement at (a) $x_{br} = 0.16$, (b) $x_{br} = 0.33$, and (c) $x_{br} = 0.5$. In all cases, $N_{br} = 13$ and the polymer concentration is $1.0c^*$. Results from simulations with HI (solid lines) and without HI (dashed lines) are shown for both combs with a single branch and linear polymers as a comparison.

shown in Fig. 5 for $n_{br} = 1$, supporting our hypothesis that local dilution expedites the relaxation of lightly branched comb polymers compared to linear polymers in semidilute solutions.

Together, these results show that comb-shaped polymers in semidilute solutions exhibit a local dilution effect, such that a small number of branches induces steric repulsion of nearby chains. For chains with long-range HI, local dilution results in more rapid relaxation. This is the predominant effect for relatively low branching density, as increasingly more branches contribute less to steric repulsion and only incur an added frictional drag.

In summary, these results highlight an unexpected trend in the relaxation behavior of comb polymers in semidilute solutions. Our results show that the dynamic behavior of nonlinear polymer chains in semidilute solutions is qualitatively different compared to dilute solutions or melts. In semidilute solutions, a complex interplay between nonlinear polymer architecture, steric interactions, and hydrodynamics results in surprising relaxation behavior that is not captured by existing theories. From this view, our work motivates the need to develop new descriptions for branched polymer dynamics, focusing on the role of concentration, molecular weight, and polymer architecture. Such interactions become increasingly complex as polymer concentration approaches the critical entanglement concentration [48], where understanding topological constraints in the presence of hydrodynamics will be critical to advance new theories for polymer solution dynamics.

This work was supported by National Science Foundation, NSF CBET 1254340 for C.M.S., NSF Grant No. CBET 1803757 for C.E.S., and a DuPont Science and Engineering Fellowship for C.D.Y.

-
- [1] T. McLeish, A tangled tale of topological fluids, *Phys. Today* **61** (8), 40 (2008).
 - [2] F. Snijkers, R. Pasquino, P. Olmsted, and D. Vlassopoulos, Perspectives on the viscoelasticity and flow behavior of entangled linear and branched polymers, *J. Phys.: Condens. Matter* **27**, 473002 (2015).
 - [3] M. Doi and S. F. Edwards, *The theory of polymer dynamics* (Oxford University Press, New York, 1988), Vol. 73.
 - [4] E. Van Ruymbeke, H. Lee, T. Chang, A. Nikopoulou, N. Hadjichristidis, F. Snijkers, and D. Vlassopoulos, Molecular rheology of branched polymers: Decoding and exploring the role of architectural dispersity through a synergy of anionic synthesis, interaction chromatography, rheometry and modeling, *Soft Matter* **10**, 4762 (2014).
 - [5] Z.-C. Yan and D. Vlassopoulos, Chain dimensions and dynamic dilution in branched polymers, *Polymer* **96**, 35 (2016).
 - [6] D. Lohse, S. T. Milner, L. Fetters, M. Xenidou, N. Hadjichristidis, R. Mendelson, C. Garcia-Franco, and M. Lyon, Well-defined, model long chain branched polyethylene. 2. Melt rheological behavior, *Macromolecules* **35**, 3066 (2002).
 - [7] J. Dealy and R. Larson, *Structure and rheology of molten polymers: From structure to flow behavior and back again* (Hanser Gardner Publications, Munich, 2006).
 - [8] M. Kapnistos, D. Vlassopoulos, J. Roovers, and L. Leal, Linear rheology of architecturally complex macromolecules: Comb polymers with linear backbones, *Macromolecules* **38**, 7852 (2005).
 - [9] D. Daniels, T. McLeish, B. Crosby, R. Young, and C. Fernyhough, Molecular rheology of comb polymer melts. 1. Linear viscoelastic response, *Macromolecules* **34**, 7025 (2001).
 - [10] F. Snijkers, D. Vlassopoulos, G. Ianniruberto, G. Marrucci, H. Lee, J. Yang, and T. Chang, Double stress overshoot in start-up of simple shear flow of entangled comb polymers, *ACS Macro Lett.* **2**, 601 (2013).
 - [11] F. Snijkers, D. Vlassopoulos, H. Lee, J. Yang, T. Chang, P. Driva, and N. Hadjichristidis, Start-up and relaxation of well-characterized comb polymers in simple shear, *J. Rheol.* **57**, 1079 (2013).
 - [12] J. W. Robinson, Y. Zhou, J. Qu, J. T. Bays, and L. Cosimbescu, Highly branched polyethylenes as lubricant viscosity and friction modifiers, *React. Funct. Polym.* **109**, 52 (2016).

- [13] X. J. Loh, *Polymers for personal care products and cosmetics* (Royal Society of Chemistry, Cambridge, UK, 2016).
- [14] G. Panzarasa, M. Dübner, G. Soliveri, M. Edler, and T. Griesser, Branched poly(ethyleneimine): A versatile scaffold for patterning polymer brushes by means of remote photocatalytic lithography, *Nanotechnology* **28**, 395302 (2017).
- [15] B. R. Sveinbjörnsson, R. A. Weitekamp, G. M. Miyake, Y. Xia, H. A. Atwater, and R. H. Grubbs, Rapid self-assembly of brush block copolymers to photonic crystals, *Proc. Natl. Acad. Sci. USA* **109**, 14332 (2012).
- [16] B. Patel, D. Walsh, D. Kim, J. Kwok, B. Lee, D. Guirounet, and Y. Diao, Tunable structural color of bottlebrush block copolymers through direct-write 3D printing from solution, *Sci. Adv.* **6**, eaaz7202 (2020).
- [17] C. M. Schroeder, Single polymer dynamics for molecular rheology, *J. Rheol.* **62**, 371 (2018).
- [18] C. M. Schroeder, R. E. Teixeira, E. S. Shaqfeh, and S. Chu, Dynamics of DNA in the flow-gradient plane of steady shear flow: Observations and simulations, *Macromolecules* **38**, 1967 (2005).
- [19] Y. Zhou and C. M. Schroeder, Dynamically Heterogeneous Relaxation of Entangled Polymer Chains, *Phys. Rev. Lett.* **120**, 267801 (2018).
- [20] R. S. Graham and R. G. Larson, Coarse-grained simulations of stretching entangled DNA using oscillating electric fields, *Chem. Commun.* **47**, 337 (2011).
- [21] M. M. Moghani and B. Khomami, Computationally efficient algorithms for Brownian dynamics simulation of long flexible macromolecules modeled as bead-rod chains, *Phys. Rev. Fluids* **2**, 023303 (2017).
- [22] C. B. Renner and P. S. Doyle, Untying knotted DNA with elongational flows, *ACS Macro Lett.* **3**, 963 (2014).
- [23] D. J. Mai, A. Saadat, B. Khomami, and C. M. Schroeder, Stretching dynamics of single comb polymers in extensional flow, *Macromolecules* **51**, 1507 (2018).
- [24] S. Li and C. M. Schroeder, Synthesis and direct observation of thermoresponsive DNA copolymers, *ACS Macro Lett.* **7**, 281 (2018).
- [25] A. R. Klotz, V. Narsimhan, B. W. Soh, and P. S. Doyle, Dynamics of DNA knots during chain relaxation, *Macromolecules* **50**, 4074 (2017).
- [26] V. Narsimhan, C. B. Renner, and P. S. Doyle, Translocation dynamics of knotted polymers under a constant or periodic external field, *Soft Matter* **12**, 5041 (2016).
- [27] K.-W. Hsiao, C. M. Schroeder, and C. E. Sing, Ring polymer dynamics are governed by a coupling between architecture and hydrodynamic interactions, *Macromolecules* **49**, 1961 (2016).
- [28] C. D. Young, J. R. Qian, M. Marvin, and C. E. Sing, Ring polymer dynamics and tumbling-stretch transitions in planar mixed flows, *Phys. Rev. E* **99**, 062502 (2019).
- [29] J. S. Hur, E. S. Shaqfeh, H. P. Babcock, D. E. Smith, and S. Chu, Dynamics of dilute and semidilute DNA solutions in the start-up of shear flow, *J. Rheol.* **45**, 421 (2001).
- [30] K.-W. Hsiao, C. Sasmal, J. Ravi Prakash, and C. M. Schroeder, Direct observation of DNA dynamics in semidilute solutions in extensional flow, *J. Rheol.* **61**, 151 (2017).
- [31] C. D. Young and C. E. Sing, Simulation of semidilute polymer solutions in planar extensional flow via conformationally averaged Brownian noise, *J. Chem. Phys.* **151**, 124907 (2019).
- [32] See Supplemental Material at <http://link.aps.org/supplemental/10.1103/PhysRevFluids.5.121301> for a detailed description of the experimental methods and computational model, supplemental figures, and supporting text.
- [33] A. B. Marciel, D. J. Mai, and C. M. Schroeder, Template-directed synthesis of structurally defined branched polymers, *Macromolecules* **48**, 1296 (2015).
- [34] M. Tanyeri and C. M. Schroeder, Manipulation and confinement of single particles using fluid flow, *Nano Lett.* **13**, 2357 (2013).
- [35] A. Shenoy, M. Tanyeri, and C. M. Schroeder, Characterizing the performance of the hydrodynamic trap using a control-based approach, *Microfluid. Nanofluid.* **18**, 1055 (2015).
- [36] A. Shenoy, C. V. Rao, and C. M. Schroeder, Stokes trap for multiplexed particle manipulation and assembly using fluidics, *Proc. Natl. Acad. Sci. USA* **113**, 3976 (2016).

- [37] A. Shenoy, D. Kumar, S. Hilgenfeldt, and C. M. Schroeder, Flow Topology During Multiplexed Particle Manipulation Using a Stokes Trap, *Phys. Rev. Appl.* **12**, 054010 (2019).
- [38] D. Kumar, A. Shenoy, S. Li, and C. M. Schroeder, Orientation control and nonlinear trajectory tracking of colloidal particles using microfluidics, *Phys. Rev. Fluids* **4**, 114203 (2019).
- [39] J. P. Berezney, A. B. Marciel, C. M. Schroeder, and O. A. Saleh, Scale-Dependent Stiffness and Internal Tension of a Model Brush Polymer, *Phys. Rev. Lett.* **119**, 127801 (2017).
- [40] K. Kremer and G. S. Grest, Dynamics of entangled linear polymer melts: A molecular-dynamics simulation, *J. Chem. Phys.* **92**, 5057 (1990).
- [41] J. Rotne and S. Prager, Variational treatment of hydrodynamic interaction in polymers, *J. Chem. Phys.* **50**, 4831 (1969).
- [42] H. Yamakawa, Transport properties of polymer chains in dilute solution: Hydrodynamic interaction, *J. Chem. Phys.* **53**, 436 (1970).
- [43] L. Miao, C. D. Young, and C. E. Sing, An iterative method for hydrodynamic interactions in Brownian dynamics simulations of polymer dynamics, *J. Chem. Phys.* **147**, 024904 (2017).
- [44] C. D. Young, M. Marvin, and C. E. Sing, Conformationally averaged iterative Brownian dynamics simulations of semidilute polymer solutions, *J. Chem. Phys.* **149**, 174904 (2018).
- [45] T. Geyer and U. Winter, An $O(N^2)$ approximation for hydrodynamic interactions in Brownian dynamics simulations, *J. Chem. Phys.* **130**, 114905 (2009).
- [46] A. Kraynik and D. Reinelt, Extensional motions of spatially periodic lattices, *Int. J. Multiphase Flow* **18**, 1045 (1992).
- [47] B. Todd and P. J. Daivis, A new algorithm for unrestricted duration nonequilibrium molecular dynamics simulations of planar elongational flow, *Comput. Phys. Commun.* **117**, 191 (1999).
- [48] Y. Zhou, K.-W. Hsiao, K. E. Regan, D. Kong, G. B. McKenna, R. M. Robertson-Anderson, and C. M. Schroeder, Effect of molecular architecture on ring polymer dynamics in semidilute linear polymer solutions, *Nat. Commun.* **10**, 1753 (2019).